Ann. Geophys., 27, 4349–4358, 2009
www.ann-geophys.net/27/4349/2009/
© Author(s) 2009. This work is distributed under
the Creative Commons Attribution 3.0 License.

Annales Geophysicae

The radial width of a Coronal Mass Ejection between 0.1 and 0.4 AU estimated from the Heliospheric Imager on STEREO

N. P. Savani[1], A. P. Rouillard[2,3], J. A. Davies[3], M. J. Owens[1], R. J. Forsyth[1], C. J. Davis[3], and R. A. Harrison[3]

[1]The Blackett Laboratory, Imperial College London, UK
[2]Space Environment Physics Group, School of Physics and Astronomy, Southampton University, Southampton, UK
[3]Space Science and Technology Department, Rutherford Appleton Laboratory, Chilton, UK

Received: 8 June 2009 – Revised: 15 November 2009 – Accepted: 16 November 2009 – Published: 30 November 2009

Abstract. On 15–17 February 2008, a CME with an approximately circular cross section was tracked through successive images obtained by the Heliospheric Imager (HI) instrument onboard the STEREO-A spacecraft. Reasoning that an idealised flux rope is cylindrical in shape with a circular cross-section, best fit circles are used to determine the radial width of the CME. As part of the process the radial velocity and longitude of propagation are determined by fits to elongation-time maps as 252±5 km/s and 70±5° respectively. With the longitude known, the radial size is calculated from the images, taking projection effects into account. The radial width of the CME, S (AU), obeys a power law with heliocentric distance, R, as the CME travels between 0.1 and 0.4 AU, such that S=0.26 $R^{0.6\pm0.1}$. The exponent value obtained is compared to published studies based on statistical surveys of in situ spacecraft observations of ICMEs between 0.3 and 1.0 AU, and general agreement is found. This paper demonstrates the new opportunities provided by HI to track the radial width of CMEs through the previously unobservable zone between the LASCO field of view and Helios in situ measurements.

Keywords. Interplanetary physics (Solar wind plasma) – Solar physics, astrophysics, and astronomy (Flares and mass ejections)

1 Introduction

Coronal mass ejections (CMEs) are large scale eruptions of plasma and magnetic fields from the solar atmosphere which propagate out into the heliosphere. Most present models postulate CMEs are initiated by a loss of equilibrium within the solar magnetic field (Forbes et al., 2006; MacNeice et al., 2004). Coronagraph observations of CMEs events have uncovered a large variability in their speed, size, and structure (St Cyr et al., 2000). Their speeds and other properties, as measured in situ by heliospheric spacecraft, also exhibit large event-to-event variability (Cane and Richardson, 2003; Richardson and Cane, 2004). Using both types of observations, CME properties have been investigated at different distances as they evolve through the heliosphere (e.g. Sheeley et al., 1985; Bothmer and Schwenn, 1996).

Various attempts have been made to classify CMEs. On the basis of their speed and acceleration profiles in coronagraph observations, CMEs have been categorized into two principle types – broadly speaking, fast CMEs typically associated with flares and type II bursts, and slow CMEs typically associated with the streamer belt and eruptive prominences (Sheeley et al., 1999). While these studies were indicative, they are by no means conclusive. This paper will concentrate on a single CME with the latter behaviour. Until recently remote observations of CMEs (and associated modelling) were limited to a maximum plane of the sky distance of 30 R_S, the field of view of the LASCO instrument on the SOHO spacecraft (Brueckner et al., 1995). CMEs are often observed to contain a typical "three part structure" consisting of an outer bright curved front, followed by a darker (less dense) inner cavity, and in turn followed by a bright core (Hundhausen, 1993). The sensitivity of the LASCO coronagraphs (Brueckner et al., 1995) is such that detailed circular striations have been observed within the cavity, suggesting the presence of a helical magnetic flux-rope structure (Dere et al., 1999). This underlying geometry has been used to identify several CMEs as "flux-rope CMEs" (Chen et al., 1997; Krall and St Cyr, 2001, 2006). Observations of magnetic flux for these structured CMEs near Earth have been used to infer that these flux-rope CMEs near the Sun are magnetically driven (Vourlidas et al., 2000). Further work has been carried out to show CMEs propagating and expanding in a self-similar manner (Cremades and Bothmer, 2004;

Correspondence to: N. P. Savani
(neel.savani@imperial.ac.uk)

Published by Copernicus Publications on behalf of the European Geosciences Union.

Cremades et al., 2006), lending itself to be modelled with a flux rope of circular cross section (Thernisien et al., 2006; Wang and Sheeley, 2006).

An abundance of observational information about CMEs is available both from coronagraph instruments, out to 30 R_S, and in situ data from various spacecraft which have explored the heliosphere beyond 0.3 AU. However there is a key observational gap in our understanding of CME evolution and propagation into interplanetary space between these two distances (Forsyth et al., 2006). Interplanetary Scintillation (IPS) (Watanabe and Schwenn, 1989) is another technique which can provide remote sensing of CMEs in this intermediary distance range. IPS provides indirect information within a wide range of distances, but there are difficulties in analysis and interpretation arising from integration along the line-of-sight. While 3-D modelling techniques for IPS have been used to deduce the density structure and velocity profiles of CMEs (Jackson et al., 2007), more detailed analysis of CME size remains problematic.

Previous in situ observational studies of the expansion properties of the interplanetary counterpart of CMEs (ICMEs) at 1 AU showed not only that radial expansion was a common feature of these transients (Klein and Burlaga, 1982; Bothmer and Schwenn, 1998; Hidalgo, 2003, 2005), but indeed, a large percentage of magnetic clouds (a subset of ICMEs identified by a specific in situ magnetic field profile) were seen to be expanding (Lepping et al., 2008). This expansion can result from a number of processes or some combination thereof. For example, an ICME may expand simply because the leading edge was ejected from the Sun at a speed greater than the trailing edge (Gosling et al., 1998; Tripathi et al., 2006). The expansion of ICMEs in the anti-sunward direction has previously been quantified using statistical surveys from multiple spacecraft over a distance range of 0.3 to 5.4 AU from the Sun (Bothmer and Schwenn, 1994; Liu et al., 2004; Wang et al., 2005). These studies have estimated the radial expansion in the form of a power law variation of CME radial width as a function of heliocentric distance. This approach does not, however, track the radial expansion of a single event, instead inferring expansion from average ICME radial extents at differing heliocentric distances. As transients have a wide range of different sizes and speeds, this leads to a large scatter in the inferred expansion. This paper takes an alternative approach by exploiting the STEREO Heliospheric Imagers to study the radial expansion of a single CME as it propagates through the field of view of the cameras. We measure the radial size of this CME between 0.14–0.41 AU, thereby filling the observational gap between coronagraph images and the closest in situ measurements to the Sun, provided by the Helios spacecraft (Schwenn, 1990).

2 Instrumentation

On 26 October 2006 (UT) the twin Solar Terrestrial Relations Observatory (STEREO) spacecraft were launched with a principle scientific objective of characterising the propagation of CMEs through the heliosphere. Both spacecraft are on Earth like orbits with one (STEREO-A) slightly closer to the Sun and thus moving ahead of Earth with a faster orbital period, and the other (STEREO-B) slightly further from the Sun and thus falling behind the Earth. Hence each spacecraft separates from the Earth at an angular rate of 22.5° per year (Russell, 2008). From 15 to 17 February 2008, the interval of interest in this paper, the two spacecraft were separated from each other by about 45.7°.

The two spacecraft carry identical instrumentation which includes the Sun-Earth Connection Coronal and Heliospheric Investigation (SECCHI) package (Howard et al., 2008). This package includes an Extreme Ultraviolet Imager (EUVI), two coronagraphs (COR1 and COR2) and the Heliospheric Imagers (HI) (Eyles et al., 2009). The HI instrument observes in visible light and contains two wide angle cameras on each STEREO spacecraft, HI-1 and HI-2; both are set to view the heliosphere from the edge of the corona with a band-pass of 630–730 nm and 400–1000 nm respectively (Harrison et al., 2005; Eyles et al., 2009). The fields of view centred at 13.7° and 53.4° elongation from the Sun and have an angular extent of 20° and 70°, respectively (elongation is the angle between the line-of-sight and the line to the Sun-centre). The HI package allows continuous tracking of solar transients from 4 degrees elongation out to Earth. The cadence of the HI-1 and 2 images are 40 min and 2 h, respectively (Eyles et al., 2009).

The HI instruments observe K-coronal electron density features from Thomson scattered sunlight. Vourlidas and Howard (2006) showed that electrons on the so-called "Thomson sphere" would contribute most effectively to the image brightness; the Sun-spacecraft line defines the diameter of this sphere. For specific solar transients to be observed from the Sun out to the Earth, the transient must spend the majority of its time travelling within the Thomson sphere created by the Sun and the spacecraft (Howard et al., 2008). The reason for this range is because a balance must be reached between the scattering angle of 90° from the Thomson affect and the inverse square drop-off rate of the scattered light intensity with increasing distance.

The typical intensity of photospheric light scattered from free electrons in the K-corona is greatly exceeded by the intensity of light scattered by the dust of the F-corona and indeed by some brighter stars (Eyles et al., 2009). In order to isolate the weak K-coronal signal a running difference technique is often used (Sheeley et al., 1997); this involves subtracting the previous image from the current one. This technique virtually eliminates the dominant F-corona signal, as the F-corona is stable over the image cadence of both cameras (Davies et al., 2009). This technique is

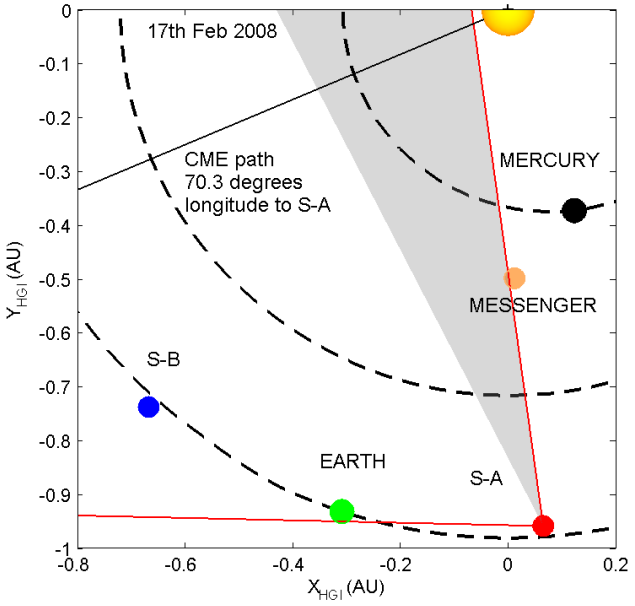

Fig. 1. The trajectories of all the spacecraft that were local to the February 2008 CME path, projected into the x-y plane in the HGI coordinate system (see main text). The orbit of Venus is displayed but the planet was positioned in another quadrant. The red lines demark the field of view of the HI cameras onboard STEREO-A, with the shaded region encompassing the field of view of HI-1.

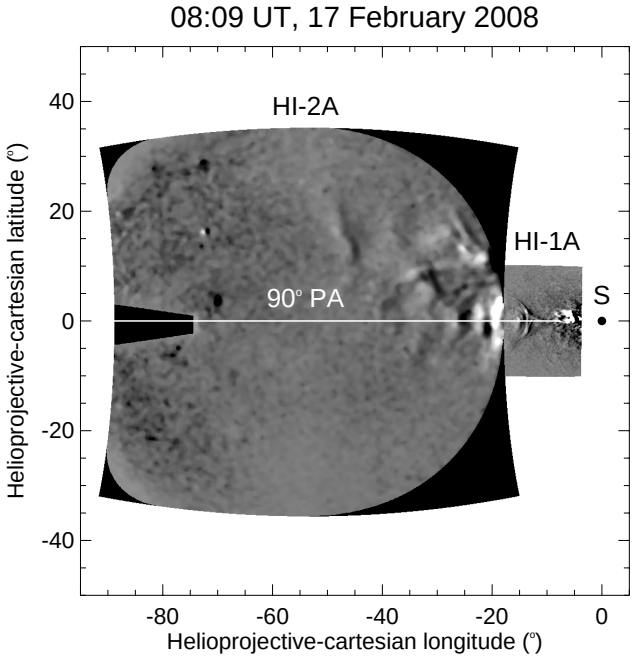

Fig. 2. A composite running difference image from the HI-1A and HI-2A cameras both taken at 08:09 UT on 17 February 2008. The transit of the CME can be observed to be passing through both cameras. These images are shown in Helioprojective Cartesian coordinates (Thompson, 2006), with a line of constant PA=90°. S marks the location of the Sun.

therefore able to both highlight the K-corona which is illuminated via Thomson scattering, and expose the density enhancement/depletion regions created by transients moving on a short time scale. Running difference images show regions of enhanced/depleted electron density relative to the previous frame as light/dark areas. As this technique may also amplify artificial changes in pixel intensity, care must be taken when considering the boundaries of "real" physical structures. This is because, for example, an observed white/ black boundary may not be exactly the trailing edge but in fact the ramping down of density within the rear boundary.

3 Observations and method

Using archived data from the STEREO HI instruments (UK solar system data centre, UKSSDC), found online at www.ukssdc.ac.uk, we carried out an initial survey of CMEs over the period of 2007–2008, seeking candidate events suitable for this study. From these results only one CME was observed to possess an approximately circular cross section, suggestive of a flux rope with an axis nearly perpendicular to the sky plane. This event entered the field of view of the HI-1 camera on STEREO-A (HI-1A) at 17:29 UT on 15 February 2008, and became too dim to track by the time it had reached the middle of the HI-2 field of view by 02:09 UT on 19 February 2008. Figure 1 shows the position of the STEREO spacecraft in the x-y plane of the heliographic inertial, HGI, coordinate system on the 17 February 2008 when the CME was observed in the centre of the HI-1 camera. The HGI coordinates are Sun-centred and inertially fixed with respect to an X-axis directed along the intersection line of the ecliptic and solar equatorial planes; the Z-axis is directed perpendicular to and northward of the solar equator, and the Y-axis completes the right-handed set (Hapgood, 1992; Thompson, 2006). During our investigation we also sought in situ observations of the CME to further constrain our assumptions. Although none were present, for the reasons of completeness the Messenger spacecraft is also displayed in Fig. 1. The estimated longitude of the CME trajectory is also shown; a full explanation on this calculation is discussed later with Fig. 3.

Figure 2 shows a typical difference image taken at 08:09 UT the 17 February 2008. The image presents the Sun at the origin, and covers the heliosphere out from the east limb of the Sun as viewed from the STEREO-A, centred about the ecliptic plane. The HI-1 camera field of view corresponds to the smaller square image closer to the Sun. At the time of this image the rear of the CME is observed in HI-1 while the front edge is beginning to enter the field of view of HI-2.

Transients observed by the HI cameras do not necessarily propagate in the plane of the sky and thus their longitude of propagation relative to the observing spacecraft must

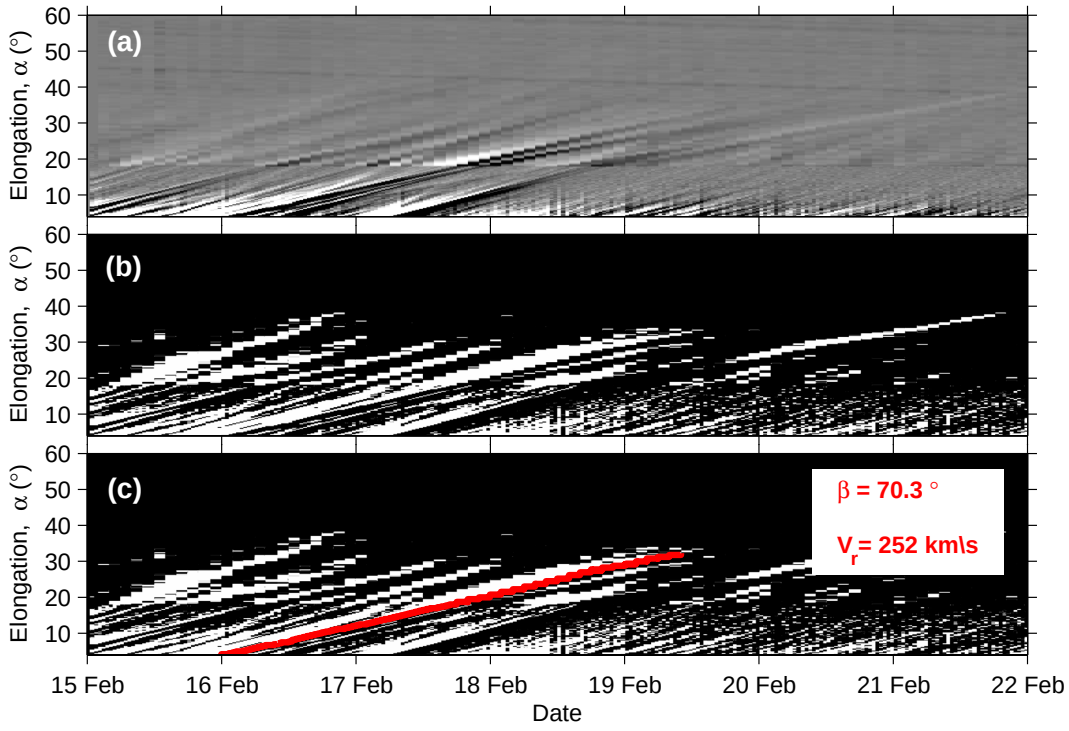

Fig. 3. (a) An elongation-time map constructed from running difference images along the equatorial line, PA=90°. **(b)** The elongation-time map converted to a binary black and white image to emphasise the tracks. **(c)** Same as b except that the additional red line is the best fit boundary of the CME. The two optimised variables from Eq. (1), longitude (β) and radial velocity (V_r), are displayed.

be inferred in order to accurately determine the distance the CME has travelled away from the Sun and to determine the true size of the CME within the image. As any solar transient moves through the HI field of view, its elongation variation exhibits an apparent acceleration/ deceleration. The form of the elongation variation depends uniquely on the radial velocity, V_r, of the transient and the observer-Sun-transient longitude, β. Sheeley et al. (2008, 2008) and Rouillard et al. (2009) have shown that the elongation variation is given by:

$$\alpha(t) = \tan^{-1}\left[\frac{V_r t \sin(\beta)}{r_A(t) - V_r t \cos(\beta)}\right] \quad (1)$$

where $\alpha(t)$ is the time varying elongation angle for a specific 'feature' in the images; and $r_A(t)$ is the heliocentric radial distance of the observer, in this case STEREO-A. Both the radial velocity and observer-Sun-transient longitude are treated as free parameters to be determined from a fit of Eq. (1) to the variation of elongation angle with time as described below.

Figure 3a shows an elongation-time map constructed from the HI-1A and HI-2A difference images during the time period of the CME, created by taking a thin slice along the equatorial plane (PA of 90°) for each image. Each slice in time is then stacked side by side such that a figure is created with time along the x-axis and elongation α on the y-axis (Davies et al., 2009). Figure 3a shows the elongation-time plots from HI-1 and 2 aligned with each other, so that continual tracking of transients could in principle be achieved to an elongation of 88°. In this format, a solar transient moving anti-sunward through the heliosphere will increase in elongation with time and thus create a sloping track that follows the density enhancement through the two fields of view.

In order to track the feature that is identified with the CME, Fig. 3a was converted from an intensity map to a binary black and white image (see Fig. 3b), by setting an arbitrary fixed value of intensity as a threshold value such that any pixel brighter than this value changed to white and any pixel darker went black. This better highlights the passage of the CME. An automated procedure was then used to trace the black/white boundary associated with the rear edge of an inner core of the CME (see Fig. 3c) to determine the elongation as a function of time. The free parameters of Eq. (1) that were a best fit to the observed elongation/time variation were calculated using an unconstrained nonlinear optimization routine based on the Nelder-Mead method (Nelder and Mead, 1965).

In order to determine the uncertainty associated with the two free parameters a second procedure was used. This was an iterative process, whereby, as one variable was kept constant at the optimal result the other was changed in small steps centred on the latter's optimal result. A profile of the

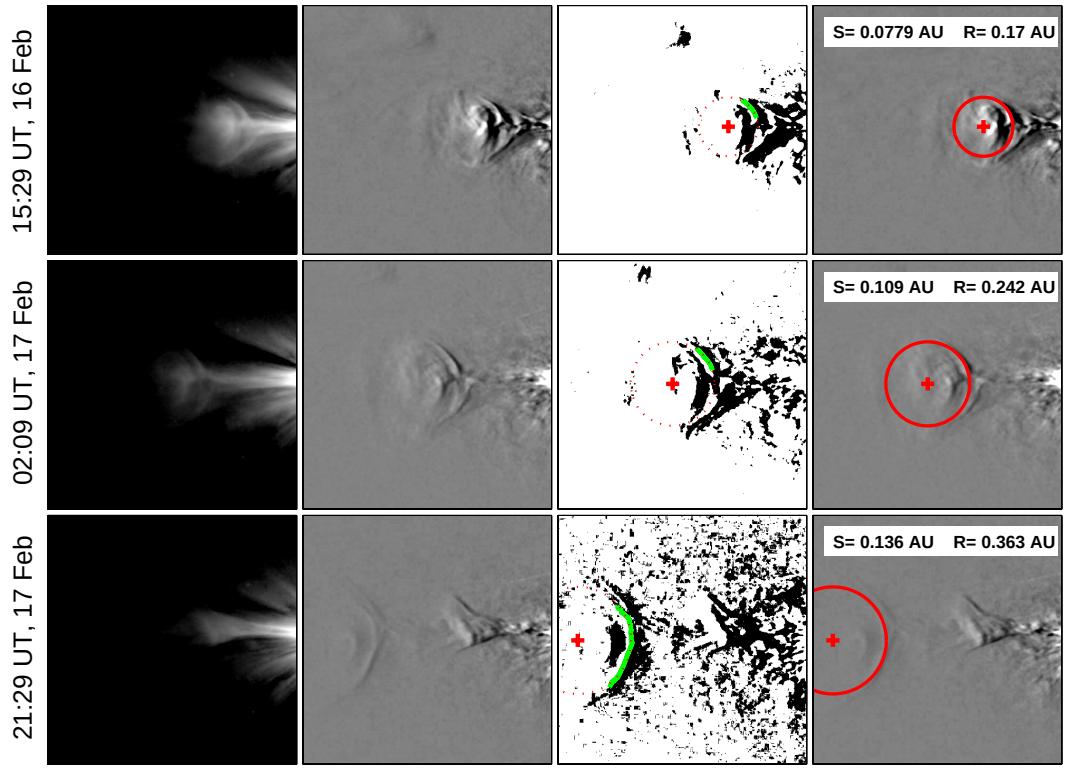

Fig. 4. (a) Left Column: Three Images from HI-1A showing the transit of the CME through the field of view. **(b)** Second Column: running difference images at the same times as those in the left column. **(c)** Third Column: the difference images converted to binary black/white. A green track is shown following the rear end of the CME, and the optimal circle shown as a red dotted line. The centre of the circle is presented as a red cross. **(d)** Right Column: displays the optimal red circle back onto the running difference images.

root mean square of the residual, obtained by taking the difference between the theoretical and observed elongation, was then generated. The full width half max (FWHM) was then calculated from this profile, from which the standard deviation, σ, was determined using Eq. (2).

$$\mathrm{FWHM} = 2\sqrt{2\ln(2)}_{\sigma} \quad (2)$$

The best fit for this track was found to be V_r=252±5 km/s and β=70±5°. Different lengths of the observed track were also tested to determine the impact on the optimised result; it was found that only including data from the HI-1 camera introduced large uncertainties due to lack of variation of the track shape over a wide range of V_r and β. Using the largest data set for the track led to the least uncertainty, thus this was the approach taken.

A clear limitation of this approach is the assumption of constant radial velocity of the CME in deriving Eq. (1). Gradual streamer CMEs tend to accelerate as they propagate out into the heliosphere (Sheeley et al., 1997; Sheeley et al., 2007). Most tracks derived from LASCO Coronagraph 3 (C3) observations fit fairly well for a constantly accelerating CME (Yashiro et al., 2004). However, most approach a constant velocity towards the outer edges of C3 located at 30 solar radii, ∼0.14 AU (Sheeley et al., 1999), which represents the position of the innermost result for this study. Analysing the velocity of a CME below 0.14 AU can also be problematic if the expansion velocity is comparable to the bulk velocity; thus we assume the core of a gradually accelerating CME achieves essentially the same speed profile as the detached transients from the tops of streamers (Sheeley et al., 1997).

The left-hand column of Fig. 4 shows HI-1 images at three different times. There is a clear density enhancement at the rear of the CME propagating out into the heliosphere. The first two also show a fainter front edge density enhancement. To analyse the orientation and shape of this concave outward structure we must consider two observational effects: firstly, the relative position of the object to the Thomson sphere and, secondly, an integration of light intensity along the line of sight.

A similar structure to that observed here has been demonstrated by simulations that scatter light from the surface of a curved, hollow tube whose ends are anchored back to the Sun. A model, cylindrical in shape with a circular cross section and plasma uniformly distributed over its surface, has been used to deduce the resulting line of sight distribution (Wang and Sheeley, 2006; Thernisien et al., 2006). It shows that if the CME propagates and expands anti-sunward with

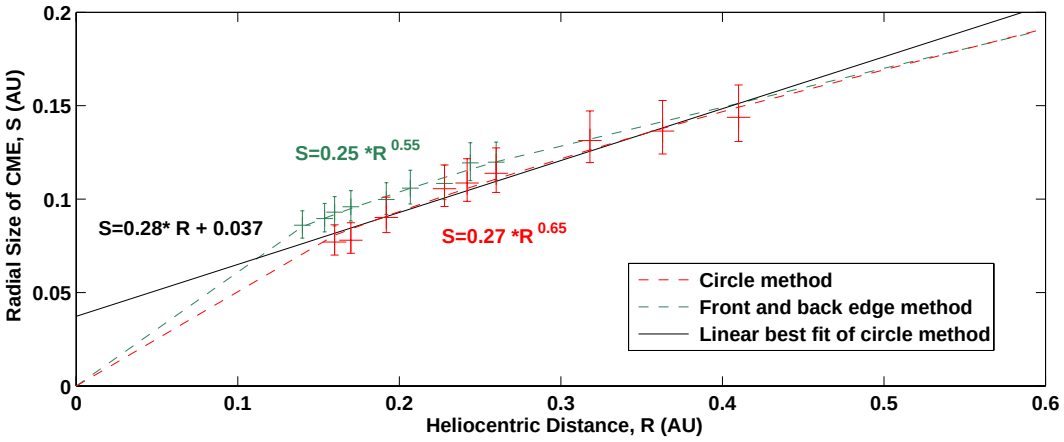

Fig. 5. Radial size of the CME versus heliocentric distance for the nine images analysed. A best fit power law for both the circular and front-rear edge methods are shown for comparison. A linear best fit to the results of the circular method is also displayed.

an axis perpendicular to the sky plane, a simulated image would display a faint circular shell, a U-shaped structure to the rear followed by an enhanced cone whose vertex remains attached to the Sun. Observationally, the CME seen in Fig. 4 appears to posses similar properties to these which lead us to consider measuring the radial width of the CME by fitting a circular profile. The elongation angle is close to the plane of sky allowing better estimation of the projection effects and justifying a simple circular representation.

The methodology used to determine the radial size of the CME as it travels anti-sunward thus consists of superimposing circular shapes onto different images at different times. For this CME the curved shape of its rear end was more clearly defined than its front. Therefore the rear of the CME was mainly used to define the circular model used. The first step in the procedure was to convert a grey scale image into a black and white image by the same method used in Fig. 3b; examples of this can be seen in Fig. 4b. The same boundary determination method used in Fig. 3c was again used to map the rear edge of the CME, shown in green in Fig. 4c. This contour was then fitted to a circle and the result overplotted in red. Figure 4d shows the circumference and the centre of the circle plotted once again on the original difference image. This method was used for nine separate images during the transit of the CME. Using the observer-Sun-transient longitude, β obtained previously, the radial size (S, measured in AU) and the heliocentric distance (R, also in AU) to the centre of the model CME were calculated (these results are displayed for the three example images in Fig. 4c).

For the boundary mapping algorithm to successfully function a clear divide between the ambient solar wind and the density enhancement must be present. Due to the effect of line of sight integration this divide is often blurred by the presence of other ejecta at possibly different longitudes. This limits the number of images that can be analysed, especially when the CME propagation is at an early stage and the ambient solar wind is more dense.

Throughout the analysed interval the circle-fitting method gives results which remain approximately consistent with the density enhancements found at the front and rear of the CME, at least for the limited period when the front edge was observable. Assuming the front edge density enhancement corresponds to the sheath region in front of a possible cylindrical flux rope (Cremades and Bothmer, 2004), then we would expect the inner edge of this density enhancement to represent the outer edge of the CME which we are trying to fit. We note that the earlier frames fit the circular shape better than the later ones, where the leading edge of the model begins to extend into the sheath region. This leads to a possible systematic error with this method. Also assuming the propagation longitude is indeed 70°, we have not included a correction for the inclination to the plane of sky which would make a circular cross section appear elliptical in the HI field of view. The error in our radial width calculation due to this effect is estimated as 9%, and is also the dominant source of uncertainty in our analysis. When comparing the radial width of a CME against the heliocentric distance travelled using a power law, the correction would change the size of the CME at each image but does not affect the exponent of the power law created.

As an alternative method for estimating the CME width, independent of the circular model, the positions of the front and rear edges were determined for nine separate images where both sides were visible. This was carried out at a PA=90°. The rear edge was defined by the density enhancement boundary and the front was defined as inside the density feature propagating out ahead of the CME.

Figure 5 displays the resulting radial widths of the CME as a function of heliospheric distance; red for the circle method; and green for the front and rear edge method. As the CME travels anti-sunward it clearly expands in the radial direction, but the rate of expansion decreases with heliocentric distance. This is evident from the systematic difference of the individual data points from a straight line fit through the data

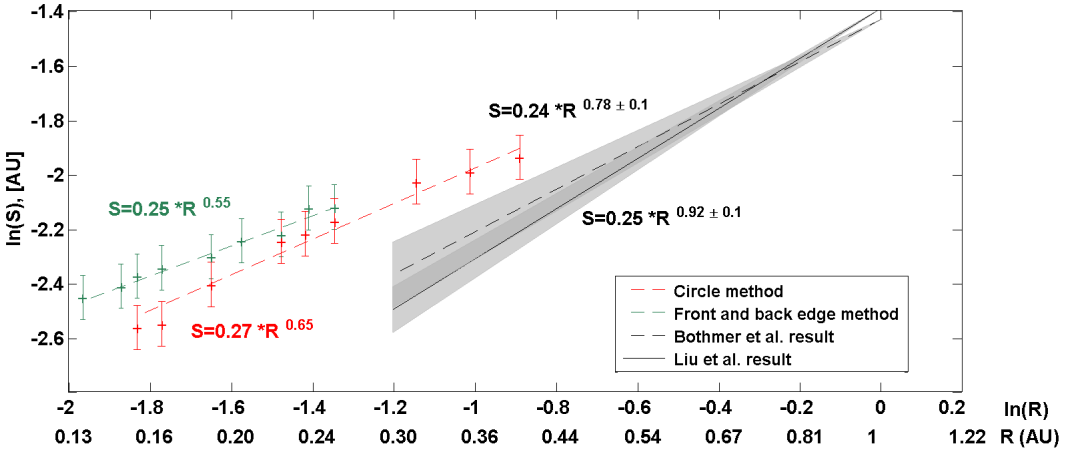

Fig. 6. A log-log plot showing the relationship between CME radial size, S, and heliocentric distance, R. The circle and front-rear edge method are compared to published statistical results in the literature from in situ observations. The grey shaded regions include the errors of the best fit curve.

generated by the circle method. Also, this best fit straight line does not pass through the origin, unrealistically implying that the CME width is 8 solar radii in the low corona. The best fit equation of this line is given by S=0.28 R+0.037, shown in black on Fig. 5.

Figure 6 compares our result from both methods to the in situ statistical surveys produced by Bothmer and Schwenn (1994) and Liu et al. (2004). The data is displayed in a log-log plot to produce a linear best fit curve. As CME radial sizes predominantly increase with increasing distance albeit at a slower rate as they progress through the heliosphere, a power law has commonly been used to depict the relationship determined from in situ observations (Bothmer and Schwenn, 1994; Wang et al., 2005). Applying power laws to our results presented in Fig. 5, both our methods give consistent results of S=0.26 $R^{0.6\pm0.1}$ within errors. This exponent value is consistent within 2 standard deviations of previous results (shown in Fig. 6) produced from statistical surveys from multiple spacecraft over 0.3–5 AU carried out by Bothmer et al. (1998) and later by Liu et al. (2004) and Wang et al. (2005) with a larger data set. A theoretical calculation was also carried out by Chen (1996) that yielded a power law with an exponent of 0.88. Our results suggest that expansion occurs at a slower rate than from previous statistical surveys, at least for this one example of a gradual streamer belt CME.

It would be prudent to consider the potential uncertainties arising from using different methods of measuring the CME size. In the statistical surveys of in situ CME observations the boundaries were determined by magnetic field data and the size was determined by multiplying the average CME velocity with the time taken for the CME to pass over the observing spacecraft. This method therefore does not take into account the effect of expansion occurring while the spacecraft is within the CME, or effects due to the axis orientation of the CME flux rope relative to the propagation direction, leading possibly to a systematic overestimate of size. Our method of directly measuring images at a fixed time is not affected by this problem. In an attempt to quantify this effect an estimate of bulk velocity and expansion speed was calculated between consecutive images. These were then used to simulate an effective radial size that would have been obtained if measured with in situ instruments on a spacecraft. It was found that the resulting power law fit made an insignificant difference within errors.

The analysis carried out in this paper is a case study of only one CME. It provides a possible new method for determining the radial expansion of CMEs, which is now available through the HI cameras on STEREO. Uncertainty in our method is compounded by using only a single CME and not having in situ data from the same CME available for comparison. It is hoped that as the archive of CMEs observed by HI builds up, a more detailed statistical approach will become possible.

4 Summary and discussion

An important target of solar and heliospheric physics has been to detect and characterise CMEs propagating through interplanetary space along the Sun-Earth line (Harrison et al., 2008). The recent launch of the STEREO spacecraft has reinvigorated the study of CMEs not least through the opportunities provided by the HI instruments. During the period of 2008 and 2009 the spacecraft have separated to optimal distances for observations where features from coronagraph images may be directly related to in situ measurements (Rouillard et al., 2008). This paper supports this goal by studying the evolution of a solar transient between 0.1–0.4 AU using the HI instruments. The main conclusions of this study can be summarised as follows:

1. The near-circular shape of this CME provided the best opportunity so far to track the radial size of a single CME beyond LASCO field of view, where the geometry allows us to better estimate possible projection effects.

2. These measurements have been taken between 0.1 and 0.4 AU. Prior to the availability of HI observations this was, apart from interplanetary scintillation techniques, an unobservable zone between coronagraphs and the closest to the Sun in situ measurements previously obtained by the Helios mission.

3. The CME studied was an example of a relatively slow, streamer belt CME during solar minimum. Its radial evolution was found to follow the power laws: S=0.25 $R^{0.65}$ and S=0.27 $R^{0.55}$ using a circular fitting and a front-rear edge separation method, respectively, with both R and S measured in AU.

4. These results indicate a possible slower expansion than indicated by in situ studies for which there are a number of possible explanations. Streamer belt CMEs may radially expand more slowly than previously indicated by in situ statistical surveys (Bothmer, 1994; Liu, 2005); or the overall speed with respect to ambient solar wind, or internal pressure of the CME may affect expansion. Perhaps if unusual solar wind conditions at the end of solar cycle 23 persist, expansion rates of CMEs may be reduced, although these conclusions have to be tempered by the fact that they are based on observations of a single event.

Although the exponent from the power law result is comparable to in-situ statistical surveys within 2 standard deviations, it nevertheless indicates that the expansion for streamer belt CMEs may be slower than the statistical surveys may suggest. This may be due to the fact that each CME has different properties such that a statistical survey may include extreme events that skew the results; or, on a larger scale, the unusual solar wind conditions for the end of solar cycle 23 (McComas et al., 2008) means the dynamic pressure and low plasma densities have noticeably reduced CMEs expansion rate. The reliability of our comparison to in situ data would be improved if our method of analysis was expanded to more CMEs.

Furthermore, the limitation of using only remote sensing observations introduces a potential systematic error. Without in situ data to confirm the start and end points of the magnetic field flux rope structure with relation to density enhancements on the images, we may have systematically over or under-estimated the CME radial width. Identifying an event that is able to combine our technique with in situ data would minimise the uncertainty and better constrain our results; as also commented by Owens (2008). Rouillard et al. (2009) have taken the first steps towards addressing this obstacle by measuring a CME from the HI cameras out to the Venus Express spacecraft; but further work is needed as a greater database of HI CME observations builds up further opportunities.

Our circular model, similar to the cross section of an idealised force free constant alpha flux rope, is a first step in monitoring radial expansion of CMEs as they propagate out from the Sun. This study may be improved by experimenting with an elliptical geometry, leading to possible understanding of the tension forces and magnetic pressure within the transient. The use of a geometrically distorted flux rope whose original shape started off as force free constant alpha cylinder (Owens et al., 2006; Owens, 2006), can potentially be used to understand these features.

Acknowledgements. STEREO/HI was developed by a consortium comprising RAL, the University of Birmingham (UK), CSL (Belgium) and NRL (USA). SECCHI, led by NRL, involves additional collaborators from LMSAL, GSFC (USA), MPI (Germany), IOTA and IAS (France). We thank E. Henley, T. S. Horbury, A. Masters and A. Rees at Imperial College London for beneficial discussions on this research topic. This work was supported by the UK Science and Technology Facilities Council (STFC).

Editor in Chief W. Kofman thanks V. Bothmer and another anonymous referee for their help in evaluating this paper.

References

Bothmer, V. and Schwenn, R.: Eruptive prominences as sources of magnetic clouds in the solar wind, Space Sci. Rev., 70(215), 215–220, 1994.

Bothmer, V. and Schwenn, R.: Signatures of Fast CMEs in Interplanetary Space, Adv. Space Res., 17, 319–322, 1996.

Bothmer, V. and Schwenn, R.: The structure and origin of magnetic clouds in the solar wind, Ann. Geophys., 16, 1–24, 1998, http://www.ann-geophys.net/16/1/1998/.

Brueckner, G. E., Howard, R. A., Koomen, M. J., Korendyke, C. M., Michels, D. J., Moses, J. D., Socker, D. G., Dere, K. P., Lamy, P. L., Llebaria, A., Bout, M. V., Schwenn, R., Simnett, G. M., Bedford, D. K., and Eyles, C. J.: The large angle spectroscopic coronagraph, Solar Phys., 162, 357–402, 1995.

Cane, H. V. and Richardson, I. G.: Interplanetary coronal mass ejections in the near-Earth solar wind during 1996–2002, J. Geophys. Res., 108(A4), 1156, doi:10.1029/2002JA009817, 2003.

Chen, J., Howard, R. A., Brueckner, G. E., Santoro, R., Krall, J., Paswaters, S. E., Stcyr, O. C., Schwenn, R., Lamy, P., and Simnett, G. M.: Evidence of an erupting magnetic flux rope: LASCO coronal mass ejection of 1997 April 13, Astrophys. Lett., 490(2), L191, 1997.

Chen, J.: Theory of prominence eruption and propagation: Interplanetary consequences, J. Geophys. Res., 1101(A12), 27499–27519, 1996.

Cremades, H. and Bothmer, V.: On the three-dimensional configuration of coronal mass ejections, Astron. Astrophys., 422(1), 307–322, 2004.

Cremades, H., Bothmer, V., and Tripathi, D.: Properties of structured coronal mass ejections in solar cycle 23, Adv. Space Res., 38(3), 461–465, 2006.

Davies, J. A., Harrison, R. A., Rouillard, A. P., Sheeley, N. R. J., Perry, C. H., Bewsher, D., Davis, C. J., Eyles, C. J., Crothers, S. R., and Brown, D. S.: A synoptic view of solar transient evolution in the inner heliosphere using the Heliospheric imagers on STEREO, Geophys. Res. Lett., 36(02), 102, doi:10.1029/2008GL036182, 2009.

Dere, K. P., Brueckner, G. E., Howard, R. A., Michels, D. J., and Delaboudiniere, J. P.: LASCO and EIT observations of helical structure in coronal mass ejections, Astrophys. J., 516(1), 465–474, 1999.

Eyles, C. J., Harrison, R. A., Davis, C. J., Waltham, N. R., Shaughnessy, B. M., Mapson-Menard, H. C. A., Bewsher, D., Crothers, S. R., Davies, J. A., Simnett, G. M., Howard, R. A., Moses, J. D., Newmark, J. S., Socker, D. G., Halain, J. P., Defise, J.-M., Mazy, E., and Rochus, P.: The Heliospheric Imagers Onboard the STEREO Mission, Solar Phys., 254(2), 387–445, 2009.

Forbes, T. G., Linker, J. A., Chen, J., Cid, C., Kota, J., Lee, M. A., Mann, G., Mikic, Z., Potgieter, M. S., Schmidt, J. M., Siscoe, G. L., Vainio, R., Antiochos, S. K., and Riley, P.: CME Theory and Models, Space Sci. Rev., 123, 251–302, 2006.

Forsyth, R. J., Bothmer, V., Cid, C., Crooker, N. U., Horbury, T. S., Kecskemety, K., Klecker, B., Linker, J. A., Odstrcil, D., Reiner, M. J., Richardson, I. G., Rodriguez-Pacheco, J., Schmidt, J. M., and Wimmer-Schweingruber, R. F.: ICMEs in the Inner Heliosphere: Origin, Evolution and Propagation Effects, Space Sci. Rev., 123(1–3), 383–416, 2006.

Gosling, J. T., Riley, P., McComas, D. J., and Pizzo, V. J.: Over-expanding coronal mass ejections at high heliographic latitudes: Observations and simulations, J. Geophys. Res., 103(A2), 1941–1954, 1998.

Hapgood, M. A.: Space Physics Coordinate Transformations – A User Guide, Planet. Space Sci., 40(5), 711–717, 1992.

Harrison, R. A., Davies, J. A., and Eyles, C. J.: The STEREO heliospheric imager: how to detect CMEs in the heliosphere, Adv. Space Res., 36(8), 1512–1523, 2005.

Harrison, R. A., Davis, C. J., Eyles, C. J., Bewsher, D., Crothers, S. R., Davies, J. A., Howard, R. A., Moses, D. J., Socker, D. G., Newmark, J. S., Halain, J. P., Defise, J.-M., Mazy, E., Rochus, P., Webb, D. F., and Simnett, G. M.: First Imaging of Coronal Mass Ejections in the Heliosphere Viewed from Outside the Sun – Earth Line, Sol. Phys., 247(1), 171–193, 2008.

Hidalgo, M. A.: A study of the expansion and distortion of the cross section of magnetic clouds in the interplanetary medium, J. Geophys. Res., 108(A8), 1320, doi:10.1029/2002JA009818, 2003.

Hidalgo, M. A.: A study of the expansion and distortion of the cross section of magnetic clouds in the interplanetary medium (vol 108, pg 1320, 2003), J. Geophys. Res., 110(A3), 110, A03207, doi:10.1029/2004JA010752, 2005.

Howard, R. A., Moses, J. D., Vourlidas, A., Newmark, J. S., Socker, D. G., Plunkett, S., Korendyke, C. M., Cook, J. W., Hurley, A., Davila, J. M., Thompson, W. T., St Cyr, O. C., Mentzell, E., Mehalick, K., Lemen, J. R., Wuelser, J. P., Duncan, D. W., Tarbell, T. D., Wolfson, C. J., Moore, A., Harrison, R. A., Waltham, N. R., Lang, J., Davis, C. J., Eyles, C. J., Mapson-Menard, H. C. A., Simnett, G. M., Halain, J. P., Defise, J.-M., Mazy, E., Rochus, P., Mercier, R., Ravet, M. F., Delmotte, F., Auchere, F., Delaboudiniere, J. P., Bothmer, V., Deutsch, W., Wang, D., Rich, N. B., Cooper, S., Stephens, V., Maahs, G., Baugh, R., McMullin, D., and Carter, T.: Sun Earth Connection Coronal and Heliospheric Investigation (SECCHI), Space Sci. Rev., 136, 67–115, 2008.

Hundhausen, A. J.: Sizes and locations of coronal mass ejections: SMM Observations from 1980 and 1984–1989, J. Geophys. Res., 98(A8), 13177–13200, 1993.

Jackson, B. V., Boyer, J. A., Hick, P. P., Buffington, A., Bisi, M. M., and Crider, D. H.: Analysis of Solar Wind Events Using Interplanetary Scintillation Remote Sensing 3D Reconstructions and Their Comparison at Mars, Solar Phys., 241(2), 385–396, 2007.

Klein, L. W. and Burlaga, L. F.: Inter-Planetary Magnetic Clouds at 1-AU, J. Geophys. Res., 87(NA2), 613–624, 1982.

Krall, J. and St Cyr, O. C.: Erupting Solar Magnetic Flux Ropes: Theory and Observation, Astrophys. J., 562(2), 1045–1057, 2001.

Krall, J. and St Cyr, O. C.: Flux-rope coronal mass ejection geometry and its relation to observed morphology, Astrophys. J., 652(2), 1740–1746, 2006.

Lepping, R. P., Wu, C.-C., Berdichevsky, D. B., and Ferguson, T.: Estimates of magnetic cloud expansion at 1 AU, Ann. Geophys., 26, 1919–1933, 2008, http://www.ann-geophys.net/26/1919/2008/.

Liu, Y., Richardson, J. D., and Belcher, J. W.: A statistical study of the properties of interplanetary coronal mass ejection from 0.3 to 5.4 AU, Planet Space Sci., 53, 3–17, 2004.

MacNeice, P., Antiochos, S. K., Phillips, A., Spicer, D. S., DeVore, C. R., and Olson, K.: A numerical study of the breakout model for coronal mass ejection initiation, Astrophys. J., 614(2), 1028–1041, 2004.

McComas, D. J., Ebert, R. W., Elliott, H. A., Goldstein, B. E., Gosling, J. T., Schwadron, N. A., and Skoug, R. M.: Weaker solar wind from the polar coronal holes and the whole Sun, Geophys. Res. Lett., 35, L18103, doi:10.1029/2008GL034351, 2008.

Nelder, J. A. and Mead, R.: A simplex method for function minimization, Comput. J., 7, 308–313, 1965.

Owens, M. J.: Magnetic cloud distortion resulting from propagation through a structured solar wind: Models and observations, J. Geophys. Res., 111(A12), 109, doi:10.1029/2006JA011903, 2006.

Owens, M. J.: Combining remote and in situ observations of coronal mass ejections to better constrain magnetic cloud reconstruction, J. Geophys. Res., 113(A12), A12102, doi:10.1029/2008JA013589, 2008.

Owens, M. J., Merkin, V. G., and Riley, P.: A kinematically distorted flux rope model for magnetic clouds, J. Geophys. Res., 111(A03), 104, doi:10.1029/2005JA011460, 2006.

Richardson, I. G. and Cane, H. V.: Identification of interplanetary coronal mass ejections at 1 AU using multiple solar wind plasma composition anomalies, J. Geophys. Res., 109, A09104, doi:10.1029/2004JA010598, 2004.

Rouillard, A. P., Davies, J. A., Forsyth, R. J., Rees, A., Davis, C. J., Harrison, R. A., Lockwood, M., Bewsher, D., Crothers, S. R., Eyles, C. J., Hapgood, M., and Perry, C. H.: First imaging of corotating interaction regions using the STEREO spacecraft, Geophys. Res. Lett., 35(L10), 110, doi:10.1029/2008GL033767, 2008.

Rouillard, A. P., Davies, J. A., Forsyth, R. J., Savani, N. P., Sheeley, N. R., Thernisien, A. F. R., Zhang, T. L., Howard, R. A., Anderson, B., Carr, C. M., Tsang, S., Lockwood, M., Davis, C. J., Harrison, R. A., Bewsher, D., Franz, M., Crothers, S. R., Eyles, C. J.,

Brown, D. S., Whittaker, I., Hapgood, M., Coates, A. J., Jones, G. H., Grande, M., Frahm, R. A., and Winningham, J. D.: A solar storm observed from the Sun to Venus using the STEREO, Venus Express, and MESSENGER spacecraft, J. Geophys. Res., 114, A07106, doi:10.1029/2008JA014034, 2009a.

Rouillard, A. P., Savani, N. P., Davies, J. A., Lavraud, B., Forsyth, R. J., Morley, S. K., Opitz, A., Sheeley, N. R., Burlaga, L. F., Sauvaud, J. A., Simunac, K. D. C., Luhmann, J. G., Galvin, A. B., Crothers, S. R., Davis, C. J., Harrison, R. A., Lockwood, M., Eyles, C. J., Bewsher, D., and Brown, D. S.: A Multispacecraft Analysis of a Small-Scale Transient Entrained by Solar Wind Streams, Solar Phys., 256(1–2), 307–326, 2009b.

Russell, C. T. (Ed.): The STEREO Mission, 136, Space Sci. Rev., Springer Netherlands, 1–646, 2008.

Schwenn, R.: Large Scale Structure of the Interplanetary Medium, Physics of the Inner Heliosphere I: Large-scale Phenomena, edited by: Schwenn, R. and Marsch, E., pp. 99–182, Springer-Verlag, Germany, 1990.

Sheeley, N. R., Howard, R. A., Koomen, M. J., Michels, D. J., Schwenn, R., Muhlhauser, K. H., and Rosenbauer, H.: Coronal Mass Ejections and Interplanetary Shocks, J. Geophys. Res, 90, 163–175, 1985.

Sheeley, N. R. J., Herbst, A. D., Palatchi, C. A., Wang, Y.-M., Howard, R. A., Moses, J. D., Vourlidas, A., Newmark, J. S., Socker, D. G., Plunkett, S. P., Korendyke, C. M., Burlaga, L. F., Davila, J. M., Thompson, W. T., St Cyr, O. C., Harrison, R. A., Davis, C. J., Eyles, C. J., Halain, J. P., Wang, D., Rich, N. B., Battams, K., and Esfandiari, E.: Heliospheric images of the solar wind at Earth, Astrophys. J., 675(675), 853–862, 2008a.

Sheeley, N. R. J., Herbst, A. D., Palatchi, C. A., Wang, Y.-M., Howard, R. A., Moses, J. D., Vourlidas, A., Newmark, J. S., Socker, D. G., Plunkett, S. P., Korendyke, C. M., Burlaga, L. F., Davila, J. M., Thompson, W. T., St Cyr, O. C., Harrison, R. A., Davis, C. J., Eyles, C. J., Halain, J. P., Wang, D., Rich, N. B., Battams, K., Esfandiari, E., and Stenborg, G.: Secchi observations of the sun's garden-hose density spiral, Astrophys. Lett., 674, L109–L112, 2008b.

Sheeley, N. R. J., Walters, J. H., Wang, Y.-M., and Howard, R. A.: Continuous tracking of coronal outflows: Two kinds of coronal mass ejections, J. Geophys. Res., 104(A11), 24739–24767, 1999.

Sheeley, N. R. J., Wang, Y.-M., Hawley, S. H., Brueckner, G. E., Dere, K. P., Howard, R. A., Koomen, M. J., Korendyke, C. M., Michels, D. J., Paswaters, S. E., Socker, D. G., St Cyr, O. C., Wang, D., Lamy, P. L., Llebaria, A., Schwenn, R., Simnett, G. M., Plunkett, S., and Biesecker, D. A.: Measurements of flow speeds in the corona between 2 and 30 solar radii, Astrophys. J., 484, 472–478, 1997.

Sheeley, N. R. J., Warren, H. P., and Wang, Y.-M.: A streamer ejection with reconnection close to the sun, Astrophys. J., 671, 926–935, 2007.

St Cyr, O. C., Howard, R. A., Sheeley, N. R. J., Plunkett, S. P., Michels, D. J., Paswaters, S. E., Koomen, M. J., Simnett, G. M., Thompson, B. J., Gurman, J. B., Schwenn, R., Webb, D. F., Hildner, E., and Lamy, P. L.: Properties of coronal mass ejections: SOHO LASCO observations from January 1996 to June 1998, J. Geophys. Res., 105(A8), 18169–18185, 2000.

Thernisien, A. F. R., Howard, R. A., and Vourlidas, A.: Modeling of flux rope coronal mass ejections, Astrophys. J., 652, 763–773, 2006.

Thompson, W. T.: Coordinate systems for solar image data, Astron. Astrophys., 449(2), 791–803, 2006.

Tripathi, D., Solanki, S. K., Schwenn, R., Bothmer, V., Mierla, M., and Stenborg, G.: Observation of a bright coronal downflow by SOHO/EIT, Astron. Astrophys., 449(1), 369–378, 2006.

Vourlidas, A. and Howard, R. A.: The Proper Treatment of Coronal Mass Ejection Brightness: A New Methodology and Implications for Observations, Astrophys. J., 642(2), 1216–1221, 2006.

Vourlidas, A., Subramanian, P., Dere, K. P., and Howard, R. A.: Large-angle spectrometric coronagraph measurements of the energetics of coronal mass ejections, Astrophys. J., 534(1), 456–467, 2000.

Wang, C., Du, D., and Richardson, J. D.: Characteristics of the interplanetary coronal mass ejections in the heliosphere between 0.3 and 5.4 AU, J. Geophys. Res., 110, A10107, doi:10.1029/2005JA011198, 2005.

Wang, Y.-M. and Sheeley, N. R. J.: Observations of flux rope formation in the outer corona, Astrophys. J., 650, 1172–1183, 2006.

Watanabe, T. and Schwenn, R.: Large-Scale Propagation Properties of Interplanetary Disturbances Revealed from IPS and Spacecraft Observations, Space Sci. Rev., 51(1–2), 147–173, 1989.

Yashiro, S., Gopalswamy, N., Michalek, G., St Cyr, O. C., Plunkett, S. P., Rich, N. B., and Howard, R. A.: A catalog of white light coronal mass ejections observed by the SOHO spacecraft, J. Geophys. Res., 109(A7), A07105, doi:10.1029/2003JA010282, 2004.